Journal of Microscopy, Vol. 194, Pt 2/3, May/june 1999, pp. 329–334.
Received 6 December 1998; accepted 30 January 1999

Femtosecond near-field scanning optical microscopy

B. A. NECHAY,* U. SIEGNER,* M. ACHERMANN,* F. MORIER-GENAUD,* A. SCHERTEL† & U. KELLER*

**Swiss Federal Institute of Technology Zurich, Institute of Quantum Electronics, ETH Hönggerberg – HPT, CH-8093 Zürich, Switzerland*

†*Micrion GmbH, Kirchenstr. 2, 85622 Feldkirchen, Germany*

Key words. Near-field optics, semiconductors, ultrafast spectroscopy.

Summary

We have developed an instrument for optically measuring carrier dynamics in thin-film materials with ≈150 nm lateral resolution, ≈250 fs temporal resolution and high sensitivity. This is accomplished by combining an ultrafast pump–probe laser spectroscopic technique with a near-field scanning optical microscope. A diffraction-limited pump and near-field probe configuration is used, with a novel detection system that allows for either two-colour or degenerate pump and probe photon energies, permitting greater measurement flexibility than that reported in earlier published work. The capabilities of this instrument are proven through near-field degenerate pump–probe studies of carrier dynamics in GaAs/AlGaAs single quantum well samples locally patterned by focused ion beam (FIB) implantation. We find that lateral carrier diffusion across the nanometre-scale FIB pattern plays a significant role in the decay of the excited carriers within ≈1 μm of the implanted stripes, an effect which could not have been resolved with a far-field system.

Introduction

Many dynamic processes in condensed matter and molecular or atomic systems take place on picosecond or subpicosecond time scales. Ultrafast optical spectroscopic techniques have yielded a wealth of information about the dynamics of electronic excitations in a variety of materials (Chergui, 1996; Shah, 1996). However, the diffraction-limited lateral resolution of conventional far-field techniques limits the physical information which can be obtained about the properties of nanometre-scale lateral structures, as their inherent inhomogeneity cannot be spatially resolved. Furthermore, far-field measurements can tell us little about the transport mechanisms on the submicrometre lateral scale. These limitations can be circumvented by measuring in the near-field with a near-field scanning optical microscope (NSOM) (Pohl *et al.*, 1984; Betzig & Trautman, 1992), which has proven useful for exploring nanometre-scale physics and chemistry in a variety of materials (Paesler & Moyer, 1996). So far, only a very few efforts to add femtosecond resolution to the NSOM (Stark *et al.*, 1995; Levy *et al.*, 1996; Vertikov *et al.*, 1996; Smith *et al.*, 1998) have been reported. This paper discusses the development of an instrument which combines a femtosecond degenerate pump-probe technique with the nanometre-scale lateral resolution of the NSOM. A novel detection system design adds measurement flexibility by allowing for both degenerate and two-colour measurements. Ultrafast measurements of carrier dynamics in nanometre-scale ion implanted single quantum well samples demonstrate the capabilities of the system (≈150 nm spatial resolution, ≈250 fs time resolution and high sensitivity) and show that information about physical processes can be obtained that is not accessible with far-field systems.

In transmission pump–probe experiments, a pump pulse excites carriers in the sample, which modify the absorption and refractive index probed by a subsequent probe pulse. The measurement of the differential probe transmission signal, i.e. the pump-induced change in the probe transmission proportional to ΔT, versus pump–probe time delay gives a measure of the dynamics of the excited carrier population. In the simplest case, this signal is proportional to the excited carrier concentration (Shah, 1996). The time resolution of such a measurement is limited only by the pump and probe pulsewidths. In most experiments, pump and probe excitations are done in the far-field – limiting the achievable lateral resolution to the diffraction limit of $\lambda/2$. However, this limitation can be circumvented by incorporating the lateral resolution of the NSOM (Pohl *et al.*, 1984; Betzig & Trautman, 1992; Paesler & Moyer, 1996),

Correspondence to: B. A. Nechay. Tel: + 41 1/633 2478; fax: 41 1/633 1059; e-mail: nechay@iqe.phys.ethz.ch

in which light is confined to a small sub-wavelength aperture that is raster-scanned across a sample in the near-field. The tip aperture size, along with the tip-sample flying height and the thickness of the active region of the sample, then determines the lateral resolution.

Experimental set-up

From various configurations combining femtosecond pump-probe techniques with the NSOM, we chose a global (far-field) pump/local (near-field) transmitted probe configuration, as shown in Fig. 1(a), mainly due to signal-to-noise considerations. The experimental set-up is shown in Fig. 1(b). The home-built NSOM instrument consists of either a pulled (Betzig & Trautman, 1992) or etched (Jiang *et al.*, 1992) NSOM tip whose aperture is held within ≈ 10 nm of the sample surface using shear-force feedback (Betzig *et al.*, 1992) with piezoelectric tuning fork detection (Karrai & Grober, 1995). Both the feedback-controlled tip-sample flying height and the sample scanning are controlled by commercial electronics. A mode-locked laser source (either a home-built Ti:sapphire or commercial Cr:LiSAF laser) generates a train of ≈ 100 fs pulses, at a wavelength of ≈ 840 nm and a repetition rate of ≈ 100 MHz, which is split into pump and probe pulses by a polarizing beam-splitter cube. The pump beam is sent through a motorized variable delay stage, which determines the time delay between the pump and probe pulses. It is then square-wave-modulated at 1 MHz by an acousto-optic modulator (AOM) before being sent up through the NSOM objective and focused onto the sample. The probe pulse is first square-wave-modulated at 1·05 MHz by an AOM and then sent through a group velocity dispersion (GVD) precompensation set-up. The resulting negatively chirped probe pulse is coupled into a single-mode NSOM fibre, emerging at the output NSOM tip aperture with pulsewidths typically below ≈ 200 fs. The output from the NSOM tip aperture is transmitted through the thin sample in the near-field and collected in the far-field through the NSOM objective to the detection optics and avalanche photodiode (APD). Finally, the differential probe transmission is measured at the 50 kHz difference frequency using a lock-in amplifier.

Issues of concern in ultrafast NSOM

In combining pump–probe spectroscopy with the NSOM various unique issues need to be considered. The most significant of these involve signal-to-noise considerations. Specifically, the differential probe transmission signal is limited not only by the very small power throughput of NSOM fibres (typically $\approx 10^{-5}$–10^{-4} W for ≈ 100 nm aperture fibres) but also by the small differential probe transmission (maximum $\Delta T/T \approx 0{\cdot}5\%$ for the samples discussed in this paper; $T =$ linear probe transmission). Furthermore, this picowatt-range signal is accompanied by large background signals, which include the transmitted probe power, which is unaffected by the pump, and the back-reflected pump power, which cannot be easily avoided with the NSOM geometry. These background signals dwarf the differential probe transmission signal. Therefore, modulation and lock-in detection are used to separate the differential probe transmission signal from the unaffected probe and back-reflected pump signals. Specifically, the nonlinear response of the sample mixes the 1·0 MHz-modulated pump and the 1·05 MHz-modulated probe signals to generate the desired differential probe transmission signal at the 50 kHz difference frequency, which is then measured with lock-in detection. The high frequencies of the pump and probe modulation reduce thermal effects of the tip–sample interaction (Rosa *et al.*, 1995) and, together with the high difference frequency, reduce the effect of laser noise.

Despite these measures, the unaffected probe and the back-reflected pump can still affect the measurement by increasing the measured shot and laser noise or even by saturating the detector. Though detection of the relatively small unaffected probe signal cannot be avoided, two measures are taken to reduce the large back-reflected pump signal. First, the pump and probe beams are orthogonally polarised so that a Glan–Thomson polariser

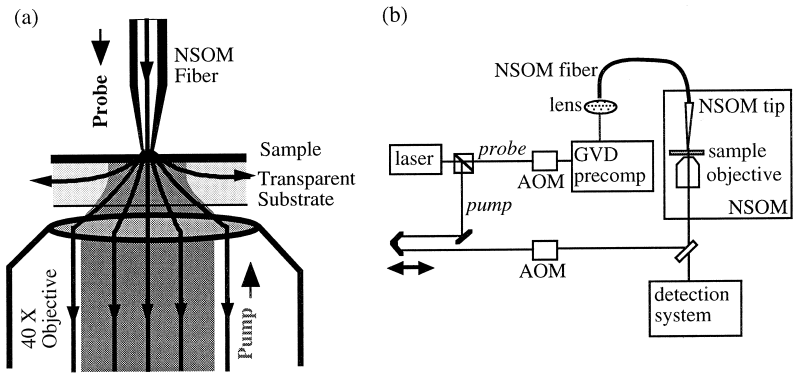

Fig. 1. (a) Global-pump, local-probe configuration; (b) experimental set-up. AOM, acousto-optic modulator; GVD, group velocity dispersion.

filters out the pump by a factor of typically more than 100, and even as high as 500, while passing most of the probe. Secondly, a confocal arrangement spatially filters out the light outside of a 1·25 μm diameter sample area, thereby reducing the back-reflected pump by as much as a factor of 100. No spectral filtering is used, allowing for degenerate pump and probe wavelengths and avoiding the need for complicated two-colour laser set-ups.

These precautions significantly improve the attainable signal-to-noise ratio of our system, allowing us to measure noise-equivalent powers (NEPs) of differential probe transmission signals typically below 1·4 pW (rms) for a 1 s lock-in time constant. For a 10 nW (rms) transmitted probe, this NEP is 1·1 pW (rms), corresponding to a sensitivity in the differential probe transmission ratio, $\Delta T/T$, of $\approx 1\times10^{-4}$.

In addition to signal-to-noise considerations, the GVD of the probe pulse in the NSOM fibre is also an important issue because this GVD broadens the probe pulsewidth, limiting the time resolution. Therefore, a standard two-prism (Duarte & Piper, 1982) GVD precompensation set-up was introduced before the fibre coupler, adding a negative GVD to the pulse that balances the positive GVD of the fibre. Measurements revealed that the pulsewidth can be largely recovered with proper GVD optimization, keeping the probe pulsewidth out of the fibre within $\approx$ 150 fs. Furthermore, at fibre input powers below the damage threshold of the NSOM tip, nonlinear effects in the fibre are so weak that the pulse spectrum is not distorted.

Lastly, topographical artefacts are a major issue of concern in most NSOM measurements (Hecht *et al.*, 1997) in which the topography of the measured surface can alter the optical image, independent of the variation in optical properties. This is of less concern in this instrument as the main physics explored involves the temporal dependence of the carrier dynamics – i.e. the temporal shape of the pump-probe scan – and how this temporal dependence varies across the sample, issues in which the topographical artefacts are not significant. However, for samples with larger topographical variations, topographical artefacts must be taken into account when interpreting spatial variations in pump–probe amplitudes and in determining spatial resolution.

Instrument performance – FIB sample results

In order to prove the capabilities of the system in terms of its performance and its usefulness for measuring interesting physics, samples needed to be measured which had a reasonably predictable lateral variation in carrier dynamics. The samples chosen were undoped 80 Å single quantum well GaAs/$Al_{0·3}Ga_{0·7}$As samples, which were mounted on glass discs and selectively etched to remove the opaque substrates, thus allowing for transmission experiments. Lateral patterning of damage on the nanometre-scale was introduced using focused ion beam (FIB) implantation (Levy *et al.*, 1996) of Ga ions at 50 keV energies. Such ion implantation is known to reduce the excitonic (Silverberg *et al.*, 1985; Smith *et al.*, 1985) and continuum (Lederer *et al.*, 1999) nonlinearity and to introduce trap states, leading to fast carrier decay times (Silverberg *et al.*, 1985; Smith *et al.*, 1985; Lambsdorff *et al.*, 1991; Delpon *et al.*, 1998; Lederer *et al.*, 1999). Two samples were measured, both using the same GaAs/$Al_{0·3}Ga_{0·7}$As quantum well structures, which varied only in their FIB implantation pattern – 200 nm implanted stripes at a $\approx 3\times10^{12}$ ions cm^{-2} dose with 400 nm spaces between stripes for sample 1, and 100 nm stripes at a $\approx 8\times10^{11}$ ions cm^{-2} dose with 2 μm spaces for sample 2. All measurements were performed at 300 K, exciting and probing at the excitonic resonance at 840 nm, with a pump fluence of $\approx 4\,\mu J\,cm^{-2}$.

Figure 2 shows a 2D image of the amplitude of the pump–probe signal at zero time delay (i.e. arbitrarily defined as the time corresponding to the maximum point of the pump–probe amplitude) and the topography across the area of sample 1. One can clearly distinguish variations in the pump–probe amplitude pattern which follow the 600 nm period of the FIB implantation pattern, where the low signals (dark regions) correspond to smaller nonlinearities expected for higher implantation doses (Lederer *et al.*, 1999). It should be noted that this pattern is not seen in the

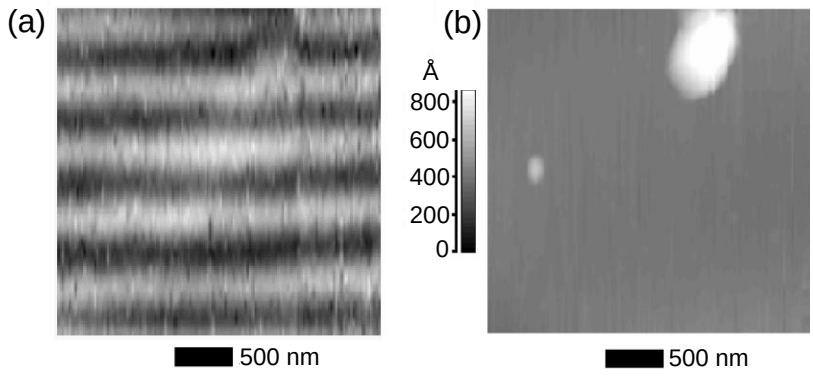

Fig. 2. Two-dimensional scans of pump–probe amplitude at zero time delay (a) and simultaneously measured topography (b) for sample 1 (GaAs/AlGaAs quantum well with 200 nm FIB implanted stripes and 400 nm spaces).

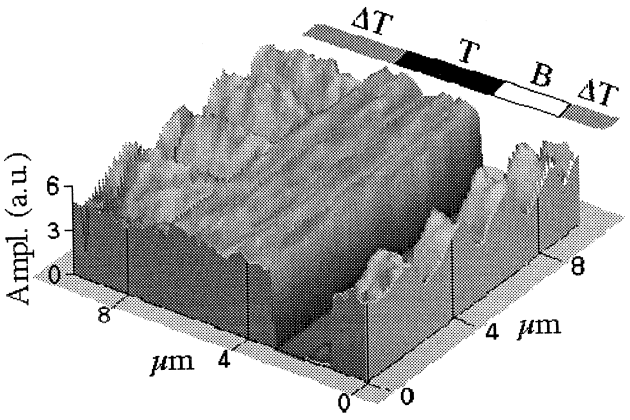

Fig. 3. Two-dimensional scan of sample 2 (GaAs/AlGaAs quantum well with 100 nm FIB implanted stripes and 2 μm spaces) where the measured optical signal is changed during the scan as shown. ΔT: differential probe transmission signal at 40 ps time delay; T: linear probe transmission, B: detector blocked.

topographical plot, proving that the measured optical pattern is not a topographical artefact (Hecht *et al.*, 1997).

One question that arises is whether these observed variations could be due to variations in the excitonic linear absorption. Indeed various effects of implantation on excitonic linear absorption have been observed (Smith *et al.*, 1985; Delpon *et al.*, 1998). To resolve this question, a 2D scan of sample 2 was taken, in which the NSOM tip was scanned across the surface of the sample while various optical signals were measured – either amplitude of the pump–probe signal (ΔT), linear probe transmission (T), or probe light blocked (B). This is shown in Fig. 3. Although the 2 μm periodicity of the implantation profile is clearly visible in the pump–probe amplitude variation, no such correlation is seen in the linear probe transmission profile, within an accuracy of the few percentage laser noise. This shows that the effect of implantation on excitonic absorption can be neglected. Therefore, it is the ultrafast nonlinear response of the sample which is measured, not the linear response.

A series of pump–probe time-domain measurements were taken at various positions across the FIB pattern of Fig. 2. Figure 4(a) shows the scan taken at position 'A', as indicated in Fig. 4(b), which shows the amplitude of these scans and their decay time versus distance across the FIB pattern. The 10–90% lateral rise in the amplitude plot of Fig. 4(b) reveals a lateral resolution as good as $\approx$ 150 nm. Indeed, this is a conservative estimate of lateral resolution as it assumes an ideal step-like variation in the implantation profile. The inset in Fig. 4(a) shows the rise of a pump–probe trace of sample 1 in which the $\approx$ 250 fs 10–90% rise time of this signal roughly represents the convolution of the sech^2-shaped $\approx$ 150 fs pump and probe pulses. This measurement shows that we can attain a time resolution of $\approx$ 250 fs.

An interesting point from Fig. 4(b) is that the decay time over the region between the stripes is relatively constant at about 8 ps, much smaller than the 100 ps recombination times measured in unimplanted areas far away from the implantation-patterned region. This effect cannot be purely due to spatial averaging of the NSOM tip or to lateral spread of the damage because the amplitude signal shows that the

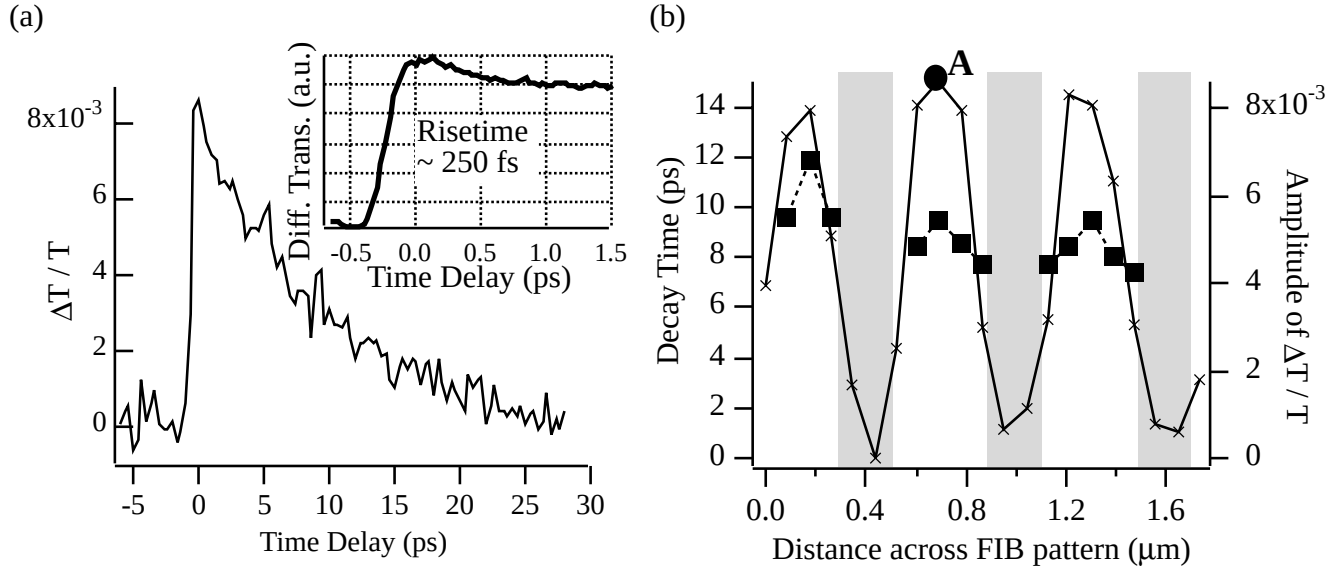

Fig. 4. (a) Pump–probe scan of sample 1 on a longer time scale; inset: pump–probe scan on a shorter time scale showing $\approx$ 250 fs time resolution. (b) Pump–probe amplitude at zero time delay (x) and decay time from a single exponential fit (■) versus distance across the sample (sample 1). The grey regions correspond to the implanted stripe.

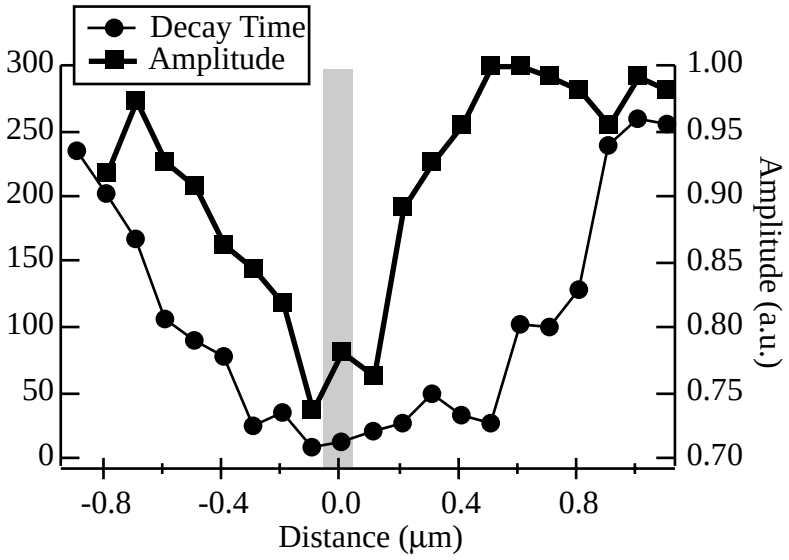

Fig. 5. Fast decay time from a double-exponential fit (●) and pump-probe amplitude at zero time delay (■) vs. distance across sample 2. The grey region corresponds to the implanted stripe.

damage is largely confined to the 200 nm implanted stripe and that variations on this length scale can be spatially resolved. Therefore, as the fast decay times cannot be explained by any local characteristic of the material, they must be the result of a non-local effect of transport. Because drift effects are expected to be insignificant, we conclude that, besides the slow recombination of electron–hole pairs, the carrier dynamics in the unimplanted regions of the sample are strongly affected by diffusion, which has also been shown to affect the decay of carriers in other types of semiconductor nanostructures (Levy *et al.*, 1996; Richter *et al.*, 1997; Smith *et al.*, 1998). Specifically, the initial excited carrier concentration is reduced at the implanted stripes due to fast trapping. The resulting concentration gradient causes carriers in the unimplanted regions to diffuse towards the implanted stripes and get trapped. Therefore, the excited carrier concentrations in the unimplanted regions are quickly depleted by this diffusion process, at a rate which is much faster than the recombination rate and which is relatively independent of the distance across the implantation pattern.

The effect of diffusion on carrier dynamics can also be seen in measurements of sample 2, whose 2 μm spacing allowed us to study carrier dynamics further away from the FIB stripe. A higher throughput, $\approx$ 300 nm aperture size NSOM tip was used here. Figure 5 shows the pump–probe amplitude and fast decay time from a double-exponential fit as a function of distance across the implantation pattern. Indeed, the decay time is roughly constant over a distance of $\approx$ 800 nm around the implanted stripe – consistent with the results seen on sample 1 – and increases to a value equal to the measured recombination time of 250 ps halfway between the implanted stripes. The spatial profile of the diffusive component of the decay time roughly follows a quadratic distance dependence (Nechay *et al.*, 1999). This is plausible because carriers excited close to the edges of the implanted stripe have a shorter distance to diffuse, resulting in enhanced diffusion, whereas diffusion of carriers excited $\approx$ 1 μm from the stripes is suppressed so that the decay in the carrier population is dominated by recombination. It is clear that the strong variation of the diffusion dynamics on a sub-micrometre scale could not have been resolved with a far-field system. These results demonstrate that the development of a femtosecond-scale time-resolved NSOM opens up new possibilities for measuring the physics of carrier dynamics in nanometre-scale structures.

Conclusion

In summary, we have developed an ultrafast NSOM, in a global-pump/local-probe configuration, with $\approx$ 150 nm lateral and $\approx$ 250 fs temporal resolution and a differential probe transmission sensitivity ($\Delta T/T$) of $\approx 10^{-4}$. By avoiding the need for spectral filtering, the detection system allows for both degenerate and two-colour measurements, thereby avoiding the need for complicated two-colour laser sources and adding greater measurement flexibility. The capabilities of this instrument have been proven through degenerate pump–probe studies of carrier dynamics in FIB implanted samples. We find that lateral diffusion effects dominate the carrier dynamics within $\approx$ 1 μm of the implanted stripes, an effect which could not have been resolved with a far-field system.

Acknowledgements

The authors acknowledge Dieter Pohl and Renato Zenobi for access to their NSOM tip fabrication facilities. This work was supported by the Swiss National Science Foundation, program NFP 36.

References

Betzig, E., Finn, P.L. & Weiner, J.S. (1992) Combined shear force and near-field scanning optical microscopy. *Appl. Phys. Lett*. **60,** 2484–2486.

Betzig, E. & Trautman, J.K. (1992). Near-field optics: microscopy, spectroscopy, and surface modification beyond the diffraction limit. *Science*, **257,** 189–195.

Chergui, M. (1996) *Femtochemistry*. World Scientific, Singapore.

Delpon, E.L., Oudar, J.L., Bouche, N., Raj, R., Shen, A., Stelmakh, N. & Lourtioz, J.M. (1998) Ultrafast excitonic saturable absorption in ion-implanted InGaAs/InAlAs multiple quantum wells. *Appl. Phys. Lett*. **72,** 759–761.

Duarte, F.J. & Piper, J.A. (1982) Dispersion theory of multiple-prism beam expanders for pulsed dye lasers. *Opt. Commun.* **43,** 303.

Hecht, B., Bielefeldt, H., Inouye, Y. & Pohl, D.W. (1997) Facts and artefacts in near-field optical microscopy. *J. Appl. Phys*. **81,** 2492–2498.

Jiang, S., Ohsawa, H., Yamada, K., Pangaribuan, T., Ohtsu, M., Imai, K. & Ikai, A. (1992) Nanometric scale biosample observation using a photon scanning tunneling microscope. *Jpn. J. Appl. Phys*. **31,** 2282–2287.

Karrai, K. & Grober, R.D. (1995) Piezoelectric tip–sample distance control for near-field optical microscopes. *Appl. Phys. Lett*. **66,** 1842–1844.

Lambsdorff, M., Kuhl, J., Rosenzweig, J., Axmann, A. & Schneider, J. (1991) Subpicosecond carrier lifetimes in radiation-damaged GaAs. *Appl. Phys. Lett*. **58,** 1881–1883.

Lederer, M.J., Luther-Davies, B., Tan, H.H., Jagadish, C., Haiml, M., Siegner, U. & Keller, U. (1999) Nonlinear optical absorption and temporal response of arsenic- and oxygen-implanted GaAs. *Appl. Phys. Lett*. **74,** 1993–1995.

Levy, J., Nikitin, V., Kikkawa, J.M., Cohen, A., Samarth, N., Garcia, R. & Awschalom, D.D. (1996) Spatiotemporal near-field spin microscopy in patterned magnetic heterostructures. *Phys Rev. Lett*. **76,** 1948–1951.

Nechay, B.A., Siegner, U., Morier-Genoud, F., Schertel, A. & Keller, U. (1999) Femtosecond near-field optical spectroscopy of implantation patterned semiconductors. *Appl. Phys. Lett*. **74,** 61–63.

Paesler, M.A. & Moyer, P.J. (1996) *Near-Field Optics: Theory, Instrumentation, and Applications*. John Wiley & Sons, Inc, New York.

Pohl, D.W., Denk, W. & Lanz, M. (1984) Optical stethoscopy: image recording with resolution lambda/20. *Appl. Phys. Lett*. **44,** 651–653.

Richter, A., Brehme, G., Süptitz, M., Lienau, C., Elsässer, T., Ramsteiner, M., Nötzel, R. & Ploog, K.H. (1997) Real-space transfer and trapping of carriers into single GaAs quantum wires studied by near-field optical spectroscopy. *Phys Rev. Lett*. **79,** 2145–2148.

Rosa, A.H., Yakobson, B.I. & Hallen, H.D. (1995) Origins and effects of thermal processes on near-field optical probes. *Appl. Phys. Lett*. **67,** 2597–2599.

Shah, J. (1996) *Ultrafast Spectroscopy of Semiconductors and Semiconductor Nanostructures*. Springer-Verlag, Berlin.

Silverberg, Y., Smith, P.W., Miller, D.A.B., Tell, B., Gossard, A.C. & Wiegmann, W. (1985) Fast nonlinear optical response from proton-bombarded multiple quantum well structures. *Appl. Phys. Lett*. **46,** 701–703.

Smith, S., Holme, N.C.R., Orr, B., Kopelman, R. & Norris, T. (1998) Ultrafast measurement in GaAs thin films using NSOM. *Ultramicroscopy*, **71,** 213–223.

Smith, P.W., Silberberg, Y. & Miller, D.A.B. (1985) Modelocking of semiconductor diode lasers using saturable excitonic nonlinearities. *J. Opt. Soc. Am. B*, **2,** 1228–1236.

Stark, J.B., Mohideen, U. & Slusher, R.E. (1995) Ultrafast near-field optical probing. *Quantum Electronics Conference 16, OSA Technical Dig. Ser. (OSA, Washington, D.C.*, p. 82.

Vertikov, A., Kuball, M., Nurmikko, A.V. & Maris, H.J. (1996) Time-resolved pump-probe experiments with subwavelength lateral resolution. *Appl. Phys. Lett*. **69,** 2465–2467.